

Triangular buckling patterns of twisted inextensible strips

BY A. P. KORTE, E. L. STAROSTIN AND G. H. M. VAN DER HEIJDEN

*Centre for Nonlinear Dynamics, University College London, London WC1E 6BT,
UK*

a.korte@ucl.ac.uk

e.starostin@ucl.ac.uk

g.heijden@ucl.ac.uk

When twisting a strip of paper or acetate under high longitudinal tension, one observes, at some critical load, a buckling of the strip into a regular triangular pattern. Very similar triangular facets have recently been observed in solutions to a new set of geometrically-exact equations describing the equilibrium shape of thin inextensible elastic strips. Here we formulate a modified boundary-value problem for these equations and construct post-buckling solutions in good agreement with the observed pattern in twisted strips. We also study the force-extension and moment-twist behaviour of these strips by varying the mode number n of triangular facets.

Keywords: twisted inextensible strip, triangular buckling pattern, calculus of variations, boundary-value problem, load-displacement behaviour

1. Introduction

When twisting a strip of paper or acetate under high longitudinal tension, one observes, at a critical load, a buckling of the strip into a regular triangular pattern (see figure 1(a)). The deformation is reversible. Sheets of paper or acetate are for practical purposes inextensible and the observed pattern, consisting of helically stacked nearly-flat triangular facets, appears to be nature's way of achieving global twisting by means of local bending and minimal stretch. This mode of buckling does not appear to have been reported in the literature. Perhaps this is because the phenomenon occurs at relatively large twisting angles and under relatively high tension (in order to suppress the more common looping instability). The buckling pattern observed has ridges running at roughly 45° angles to the centreline of the strip. The ridges radiate out from vertices on the edge of the strip where stress concentration occurs. There is superficial similarity with the well-known Yoshimura or diamond buckling pattern of thin cylindrical shells (Yoshimura 1930) but this pattern requires compressive rather than tensile loading.

The phenomenon of buckling of an *extensible* elastic strip under tension and twisting moment has been studied before. In the 1930s Green considered buckling of twisted strips under constant tensile force, treating both the case of zero and non-zero end force (Green 1936, Green 1937). Buckling of a twisted orthotropic plate into a sinusoidal buckling pattern in the longitudinal direction was studied in Crispino & Benson (1986). A numerical investigation of wrinkling of twisted plates

was carried in Mockensturm (2001), considering both the case of constant end-to-end distance and the case of constant end force, and finding different results in the two cases. In the latter case it was found that buckling may occur in both the lateral and longitudinal directions.

A perturbation method was used recently to further explore the wrinkling instability under small twist (Coman & Bassom 2008). As the twist increases from zero, the surface of a strip first becomes helicoidal, which causes extensional forces near the edges while the core domain is in compression. When a critical twist and tension are reached, the core domain of the strip buckles into an oscillatory pattern. The surface near the edges remains helicoidal; no strain localisation occurs.

The problem of bending and twisting of an *inextensible* flat plate has also been studied before. Such a plate deforms isometrically and its surface is therefore developable (i.e., has zero Gaussian curvature), making the analysis more geometrical. Sadowsky developed a large-deformation theory of narrow elastic strips as early as in 1930 (Sadowsky 1931). Approximate equations for wide strips were derived in the mid-1950s by Mansfield (see Mansfield 1989). These equations predict the distribution of generators of the developable surface while ignoring the actual three-dimensional geometry. This work was followed up by Ashwell (1962), where localisation of stresses at two diagonally opposite corners is found for a strip in its first buckling mode. The actual shape of the strip was not computed.

The constraint of zero Gaussian curvature causes the buckling patterns of inextensible strips to differ strongly from the oscillatory buckling patterns of extensible strips. The helicoidal shape of the edges of the strip found in Coman & Bassom (2008) is not a solution for inextensible strips not even for infinitesimally small twist. Rather we observe a sequence of relatively flat triangular domains which are not restricted to the core of the strip. The edges show a sequence of points with high curvature.

It is worth noting that both responses, the smooth sinusoidal one and the localised one, can be observed on the same paper strip model depending on the environmental conditions. When the humidity is low and the paper is dry it behaves like an inextensible material. When it is slightly wet it becomes noticeably stretchable. Note also that the solution for a slightly extensible strip is well described by the inextensible model almost everywhere except for small domains where the stress concentrates. In this paper we compute geometrically-exact developable solutions of inextensible strips.

A geometrically-exact set of equilibrium equations for the large deformation of thin inextensible plates of finite width has recently been derived (Starostin & van der Heijden 2007). The equations are ordinary differential equations and obtained by using the inextensibility constraint to reduce stresses and strains to the centreline of the strip. They are much easier to analyse than the usual partial differential equations of elastic plate theory. The new set of equations was used to solve a classical problem in mechanics, namely to find the equilibrium shape of a developable Möbius strip (Starostin & van der Heijden 2007). Numerical solutions revealed the existence, for any aspect ratio of the strip, of a nearly flat triangular region associated with the (unique) inflection point of the strip (see figure 1(b)). The triangular facet of the Möbius strip solution clearly resembles the facets of the buckling pattern of the twisted strip in figure 1(a) and in this paper we use the new system of equations to construct post-buckling solutions in good agreement

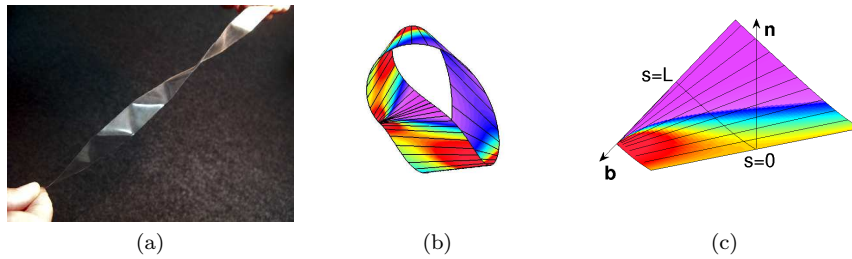


Figure 1: (a) Twisted acetate model strip under tension. (b) Möbius developable structure of aspect ratio 2π with generators shown. (c) Trapezoidal segment taken from the Möbius structure to construct the periodic strip, with normal, binormal and centreline shown, $\eta'(0) = 0, \eta(L) = 0$. The colouring changes according to the local bending energy density, from violet for regions of low bending to red for regions of high bending. Note the singularity on the edge of the strip.

with experiment. The central idea is to modify the boundary-value problem for the Möbius strip such as to ‘cut out’ the triangular (more precisely, trapezoidal) region (see figure 1(c)) and to use symmetry to reflect and multiply the elementary triangular facet into a periodic triangular pattern. This procedure avoids having to integrate numerically through the bending energy singularity associated with the vertex of the triangle on the edge of the strip, as found in Starostin & van der Heijden (2007) and analysed further in Hornung (2009).

Having obtained a post-buckling strip solution with a certain number, say n , of triangular facets we then study the strip’s force-extension and moment-twist behaviour for various mode numbers n . Neither gravity nor other distributed forces acting on the strip are taken into account in the present work.

The paper is organised as follows. In Section 2 we formulate the boundary-value problem for the centreline-reduced equations for a developable strip. We also use symmetry properties of the solution to construct triangular buckling patterns for the strip by concatenating elementary facets. In Section 3 we numerically solve the boundary-value problem and compute load-displacement curves for the post-buckling strip solutions for various mode numbers n . In Section 4 we discuss our results and draw some conclusions.

2. The boundary-value problem

A sufficiently thin elastic surface will deform by bending only (Witten 2007) and therefore deform isometrically. If such a surface is flat in its unstressed state it will remain so under deformation and therefore have zero Gaussian curvature (Graustein 1966). It is said to be developable.

Now consider a rectangular sheet or strip. If $\mathbf{r}(s)$ is a parametrisation of the centreline of the strip, s being arclength, then

$$\begin{aligned} \mathbf{x}(s, t) &= \mathbf{r}(s) + t [\mathbf{b}(s) + \eta(s)\mathbf{t}(s)], \\ \tau(s) &= \eta(s)\kappa(s), \quad s \in [0, l], \quad t \in [-w, w] \end{aligned} \quad (2.1)$$

is a parametrisation of an embedded developable strip of length l and width $2w$ (Randrup & Røgen 1996). Here \mathbf{t} and \mathbf{b} are two unit vectors of the Frenet frame

$\{\mathbf{t}, \mathbf{n}, \mathbf{b}\}$ of tangent, principal normal and binormal to the centreline, while κ and τ are, respectively, the curvature and torsion of the centreline, which uniquely specify (up to Euclidean motions) the centreline of the strip (Graustein 1966). By equation (2.1), the surface, in turn, is completely determined by the centreline of the structure. The straight lines $s = \text{const.}$ are the generators of the surface, which make an angle $\arctan(1/\eta)$ with the positive tangent direction. Given this parametrisation, the mean curvature M can be easily calculated, e.g., by using the coefficients of the first and second fundamental forms of the surface, themselves calculated from partial derivatives of \mathbf{x} with respect to s and t (Graustein 1966). The result is

$$M = -\frac{\kappa}{2} \frac{1 + \eta^2}{1 + t\eta'}, \quad (2.2)$$

where the prime denotes differentiation with respect to arclength s .

Introducing rectangular co-ordinates (u_1, u_2) by developing the surface into a rectangle,

$$u_1 = s + t\eta(s), \quad u_2 = t, \quad (2.3)$$

the bending energy of a strip of thickness $2h$ can be written as the following integral over the surface of the strip (Love 1927):

$$U = 2D \iint M^2 du_1 du_2, \quad (2.4)$$

where $D = 2Eh^3/[3(1 - \nu^2)]$ is the flexural rigidity, E is Young's modulus and ν is Poisson's ratio. When M (given by (2.2)) is substituted into (2.4), and the co-ordinates changed to s, t , the t integration can be carried out (Wunderlich 1962) giving

$$U = Dw \int_0^L g(\kappa, \eta, \eta') ds, \quad (2.5)$$

with

$$g(\kappa, \eta, \eta') = \kappa^2 (1 + \eta^2)^2 \frac{1}{2w\eta'} \log \left(\frac{1 + w\eta'}{1 - w\eta'} \right). \quad (2.6)$$

In the zero-width limit, $w \rightarrow 0$, this reduces to the Sadowsky result $g = \kappa^2(1 + \eta^2)^2$ (Sadowsky 1931).

Minimisation of this elastic energy functional is a one-dimensional variational problem cast in a form that is invariant under Euclidean motions. In Anderson (1989) Euler-Lagrange equations for such geometric variational problems are derived in a general context via a splitting of the cotangent bundle T^*J^∞ of the infinite jet bundle J^∞ of a fibred manifold, which induces a bigrading of the differential forms on J^∞ known as the variational bicomplex (see also Kogan & Olver 2003). In more physical terms they can be written in the form of six balance equations for the (normalised) components of the internal force, $\mathbf{F} = (F_t, F_n, F_b)^T$, and moment, $\mathbf{M} = (M_t, M_n, M_b)^T$, in the directions of the Frenet frame, and two scalar equations (Starostin & van der Heijden 2007, Starostin & van der Heijden 2009):

$$\mathbf{F}' + \boldsymbol{\omega} \times \mathbf{F} = \mathbf{0}, \quad \mathbf{M}' + \boldsymbol{\omega} \times \mathbf{M} + \mathbf{t} \times \mathbf{F} = \mathbf{0}, \quad (2.7)$$

$$\partial_\kappa g + \eta M_t + M_b = 0, \quad (\partial_{\eta'} g)' - \partial_\eta g - \kappa M_t = 0, \quad (2.8)$$

where $\boldsymbol{\omega} = \kappa(\eta, 0, 1)^T$ is the Darboux vector. The equations (2.7) are nothing but the vectorial fixed-frame force and moment balance equations $\mathbf{F}' = \mathbf{0}$, $\mathbf{M}' + \mathbf{r}' \times \mathbf{F} = \mathbf{0}$, written out in the Frenet frame. (Here we adopt the convention that bold roman symbols are used for vectors while bold italic symbols are used for triples of components of these vectors in the Frenet frame.) It follows immediately that $\mathbf{F} \cdot \mathbf{F}$ and $\mathbf{M} \cdot \mathbf{F}$ are first integrals of the equations. Note that the first equation in (2.8) is algebraic in the variables (κ, η, η') , while the second is a second-order ordinary differential equation (ODE) in η .

It will be of interest to a more general audience how the same equations can be obtained from first principles using standard variational methods, extending to a function of κ, τ, κ' and τ' the examples in Capovilla *et al.* (2002) (which covers functional dependence up to κ, τ only). This is done in the appendix, where it is shown that it is straightforward to accommodate the additional functional dependence on κ', τ' without computing any new variations, by simply reusing the results already given in Capovilla *et al.* (2002) and Langer & Perline (1991). The additional terms generated by the dependence of g on κ' and τ' are easily managed. It is straightforward to extend this method to a functional involving any number of derivatives of κ and τ , and hence obtain the closed-form expressions given in Starostin & van der Heijden (2009).

The shape of the strip's centreline is found by first differentiating the first equation in (2.8) in order to turn it into a differential equation and then numerically solving equations (2.7) and (2.8) as a boundary-value problem (BVP) in conjunction with three Euler-angle equations describing the evolution of the Frenet frame relative to a fixed frame, and the centreline equation $\mathbf{r}' = \mathbf{t}$. Taking Love's convention for the Euler angles (θ, ψ, ϕ) (Love 1927), the derivatives of the angles are related to the curvature and torsion as

$$\begin{aligned}\theta' &= \kappa \cos \phi, \\ \psi' &= \kappa \sin \phi / \sin \theta, \\ \phi' &= -\kappa \sin \phi \cot \theta + \kappa \eta,\end{aligned}\tag{2.9}$$

while the centreline equation in component form gives

$$\begin{aligned}x' &= \sin \theta \cos \psi, \\ y' &= \sin \theta \sin \psi, \\ z' &= \cos \theta.\end{aligned}\tag{2.10}$$

Equation (2.9) can be written down directly from the Darboux vector by noting that Love's convention is the usual y -convention (van der Heijden & Thompson 2000) in classical mechanics with ψ and ϕ interchanged (Goldstein 1980). Alternatively it can be obtained from the Frenet-Serret equations. The convention is such that the polar singularity (here at $\theta = 0$) usually associated with Euler angles does not cause any problems for the solutions we are interested in (the flat strip will have $\theta = \pi/2$). Alternatively a 4-parameter quaternion representation can be used to avoid the singularity at the expense of a norm condition.

Before we specify the boundary conditions let's have a closer look at the buckling pattern in figure 1(a) and the Möbius strip solution in figure 1(b). The Möbius strip solution has special points where either η or η' is zero. Points where $\eta' = 0$ are called

cylindrical points as the surface is locally a cylinder, i.e., the mean curvature in (2.2) is constant along the local generator. In figure 1(b) this corresponds to a generator of constant colour. Points where $\eta = 0$, by contrast, are called conical because the edge of regression, on which nearby generators intersect each other, has a cusp. At these conical points the generator is perpendicular to the centreline, as follows from (2.1). Clearly there must be at least one point where $\eta' = 0$ between any two points with $\eta = 0$. In fact, the Möbius strip has three cylindrical points and three conical points, one of the latter being special because it corresponds to the only inflection point of the centreline (where $\kappa = 0$). At this point the binormal component of both the force and the moment are zero. Furthermore it is found that at the inflection point, $|\eta'| \rightarrow 1/w$ (i.e., the edge of regression reaches the edge of the strip) and the bending energy density g diverges, i.e., we have stress concentration. As is seen in figure 1(b), coming out of this singular point is a nearly flat (violet) triangular region.

Now, turning to figure 1(a) we observe that the buckling pattern consists of points of high stress located alternately on both edges of the strip, while locally cylindrical ridges bound flat triangular (more precisely, trapezoidal) regions similar to those found in the Möbius strip solution. This suggests that we can describe the buckling pattern by a solution of the equations built up of alternating copies of the trapezoidal section between the inflection point (where $\eta = 0$) and the nearest cylindrical point (where $\eta' = 0$). A cut-out of this section is shown in figure 1(c). Note that both bounding generators are of constant colour, illustrating that the section can be reflected about both end generators.

A two-step symmetry operation is therefore used to construct a strip of length $2nL$ from a trapezoid of length L . Let the arclength parameter of the centreline be $s = 0$ at the cylindrical point ($\eta' = 0$) and $s = L$ at the inflection point ($\eta = 0$) (see figure 1(c)). The first operation is a rotation through 180° of the trapezoid about the normal \mathbf{n}_1 at $s = 0$ (see also figure 2). The original and the rotated trapezoid together make a continuous surface, which forms one period of the full strip (P_1 of figure 2), of length $2L$. The binormal to the strip at the inflection point is denoted \mathbf{b}_0 .

In the second step a symmetrical strip of $n + 1$ periods is obtained from a parent strip of n periods by rotating an end period of the parent strip 180° about the end binormal. This binormal is located at the inflection point of that end period and therefore aligned with the end generator. Thus strips of any period can be built up in this way by successively reflecting an end period about its end binormal. The length of the centreline of a symmetrical strip of n periods made in this way is therefore $2nL$. In particular, let $\mathbf{r}(0) \equiv \mathbf{r}_0$, $\mathbf{r}(L) \equiv \mathbf{r}_1$ be respectively the position vectors of the centreline at the inflection and cylindrical points of the trapezoid solution of the BVP. Define a rotation of π around the unit vector \mathbf{g} ,

$$R_{\mathbf{g}}(\mathbf{a}) = 2\mathbf{g}(\mathbf{g} \cdot \mathbf{a}) - \mathbf{a}, \quad (2.11)$$

then the first and subsequent periods are obtained by the iteration

$$\begin{aligned} \mathbf{r}_2 &= \mathbf{r}_1 + R_{\mathbf{n}_1}(\mathbf{r}_0 - \mathbf{r}_1), & \mathbf{b}_2 &= R_{\mathbf{n}_1}(\mathbf{b}_0), \\ \mathbf{r}_{2i} &= \mathbf{r}_{2i-2} + R_{\mathbf{b}_{2i-2}}(\mathbf{r}_{2i-4} - \mathbf{r}_{2i-2}), & \mathbf{b}_{2i} &= R_{\mathbf{b}_{2i-2}}(\mathbf{b}_{2i-4}), \end{aligned} \quad (2.12)$$

where $i = 2, \dots, n$. The \mathbf{b}_{2i} are then the unit binormals at the inflection points of the periods of the strip. The reflection rules in (2.12) are for the centreline, but

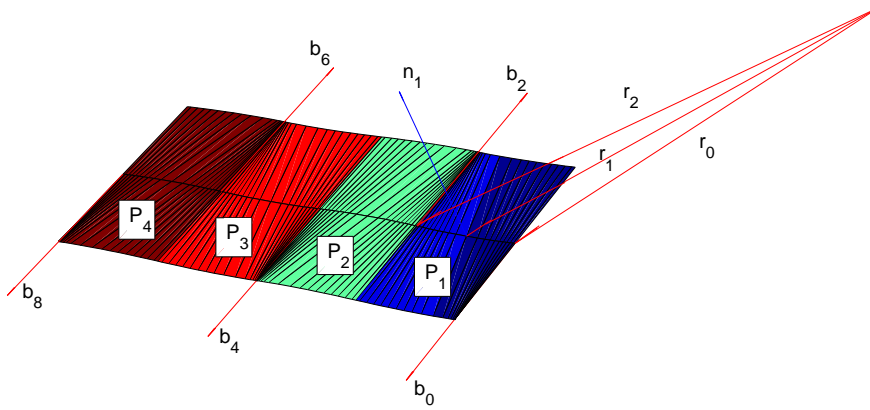


Figure 2: Mode $n = 4$ symmetry operations. The first half period is rotated about \mathbf{n}_1 to form the first period P_1 . Rotating P_1 about \mathbf{b}_2 produces the second period P_2 . Rotating P_2 about \mathbf{b}_4 , then P_3 about \mathbf{b}_6 , produces the final two periods of the figure.

can be easily generalised to the whole surface, as was done in Starostin & van der Heijden (2007) to obtain closed-strip solutions from the trapezoid solution of the BVP. These reflection rules are shown in figure 2 for the example $n = 4$ with the relevant binormals shown. The initial trapezoid (with one boundary aligned with \mathbf{b}_0) is rotated about \mathbf{n}_1 giving the first period P_1 . This first period is then rotated about \mathbf{b}_2 to give the second period P_2 , which itself is rotated about \mathbf{b}_4 to give the third period P_3 . Finally the third period is rotated about \mathbf{b}_6 to give the fourth period P_4 .

It remains to formulate the boundary conditions for the initial trapezoid. At $s = 0$ these are

$$\begin{aligned} F_n(0) &= 0, & M_n(0) &= 0, & \eta'(0) &= 0, \\ x(0) &= 0, & y(0) &= 0, & z(0) &= 0, \end{aligned} \quad (2.13)$$

where the values for x , y and z fix an arbitrary position in space, and

$$M_b(0) = -\eta(0)M_t(0) - 2\kappa(0)(1 + \eta^2(0))^2, \quad (2.14)$$

which can be read off as the $s = 0$ limit of the first equation of (2.8), where $\eta'(0) = 0$. Equation (2.14) is required to fix the integration constant for the ODE obtained by differentiating the first equation of (2.8). (Note that by Taylor expanding the second of equations (2.8) around $s = 0$, one can also show that $M_t(0) = \frac{2}{3}(1 + \eta^2(0))\kappa(0)(-6\eta(0) + w^2(1 + \eta^2(0))\eta''(0))$).

The boundary conditions at $s = L$ are

$$\begin{aligned} \kappa(L) &= 0, & F_b(L) &= 0, & M_b(L) &= 0, \\ \theta(L) &= \pi/2, & \psi(L) &= 0, & \phi(L) &= \pi, \end{aligned} \quad (2.15)$$

where the angles fix an arbitrary orientation of the strip in space.

The force and moment boundary conditions in (2.13) and (2.15) are enforced by the rotational symmetry. Since \mathbf{n}_1 and \mathbf{b}_0 are local axes of rotational (or reflection) symmetry, any component of force and moment along those axes must vanish. This

guarantees continuity of forces and moments in the strip and therefore yields a valid solution of the mechanical problem.

The remaining boundary conditions for the system of ODEs are the projections of the end force and moment of the strip on the end-to-end unit vector $\hat{\mathbf{e}} = \mathbf{e}/|\mathbf{e}|$, $\mathbf{e} = \mathbf{r}_{2n} - \mathbf{r}_0$,

$$\mathbf{F}(L) \cdot \hat{\mathbf{e}} = \bar{F}, \quad \mathbf{M}(L) \cdot \hat{\mathbf{e}} = \bar{M}, \quad (2.16)$$

where \bar{F}, \bar{M} are also continuation (control) parameters. Equations (2.13)–(2.16) give a final count of 15 boundary conditions for the same number of first-order ODEs.

The BVP is solved by continuation of each of the boundary conditions in (2.16) in turn. To obtain the starting solution of the continuation, the numerical solution of the Möbius strip between the inflection point and nearest cylindrical point is continued in $F_n(0)$ and $M_n(0)$ until equations (2.13) are satisfied.

There are significant numerical difficulties solving this BVP as both ends of the integration interval have a singularity. The boundary condition $\kappa(L) = 0$ enforces an inflection point at $x = L$. At this point the torsion τ must also be zero and in fact it must go to zero, in s , faster than the curvature κ (Randrup & Røgen 1996). Therefore we also have $\eta(L) = 0$. In practice, to compute a starting solution we first compute an approximate solution with $\kappa(L) \simeq 0.1$ to stay away from the singularity at $x = L$. When all other boundary conditions are satisfied we ‘pull’ the solution into the singularity by continuing $\kappa(L)$ to zero as far as possible, typically reaching values of 0.001. At this point we typically have $\eta(L) \simeq 0.002$, while $|\eta'(L)| - 1/w$, the distance from the singularity, is typically as small as 10^{-6} .

At the other singularity, at $s = 0$, numerical convergence requires Taylor expansions (up to fourth order in our case) of the left-hand sides of equations (2.8) about $\eta' = 0$ to be used for a small interval around $s = 0$. In addition, to improve convergence, the absolute value of the logarithm is taken in equation (2.6). We note that it has not proved possible (for instance by similar Taylor expansions) to remove the singularity in (2.8) at $\eta' = 1/w$.

As a check on the numerical results, the first integrals $\mathbf{F} \cdot \mathbf{F}$ and $\mathbf{M} \cdot \mathbf{F}$ are typically found to be constant to within 10^{-9} .

Once the BVP has been solved, the surface of the strip is obtained from (2.1) and the reflection rules (2.12). We note that no measures in the above formulation are taken to prevent self-intersection of the strip.

3. Numerical results: response of the strip to applied loads

The AUTO continuation software (Doedel *et al.* 2007) was used to compute response curves of applied force $\bar{F} \equiv \mathbf{F}(L) \cdot \hat{\mathbf{e}}$ against end-to-end distance of the strip $|\mathbf{e}|$, and applied moment $\bar{M} \equiv \mathbf{M}(L) \cdot \hat{\mathbf{e}}$ against the accumulated twist angle α . As the component of \mathbf{b}_0 perpendicular to \mathbf{e} is $\mathbf{a}_0 \equiv \mathbf{b}_0 - (\mathbf{b}_0 \cdot \hat{\mathbf{e}})\hat{\mathbf{e}}$, with \mathbf{a}_{2n} similarly defined, the twist angle α is the angle between the components of the two end-of-strip binormals perpendicular to the end-to-end vector of the strip, and therefore $\cos \alpha = \mathbf{a}_0 \cdot \mathbf{a}_{2n} / (|\mathbf{a}_0||\mathbf{a}_{2n}|)$.

Under a distance rescaling $s \rightarrow s' = sk$, the force and moment scale as $\mathbf{F} \rightarrow \mathbf{F}/k^2$ and $\mathbf{M} \rightarrow \mathbf{M}/k$ (\mathbf{M} scales as κ , cf. equation (2.14)), κ scales as $\kappa \rightarrow \kappa/k$, whereas η and the Euler angles are scale invariant. Rescaling can be used to obtain strip

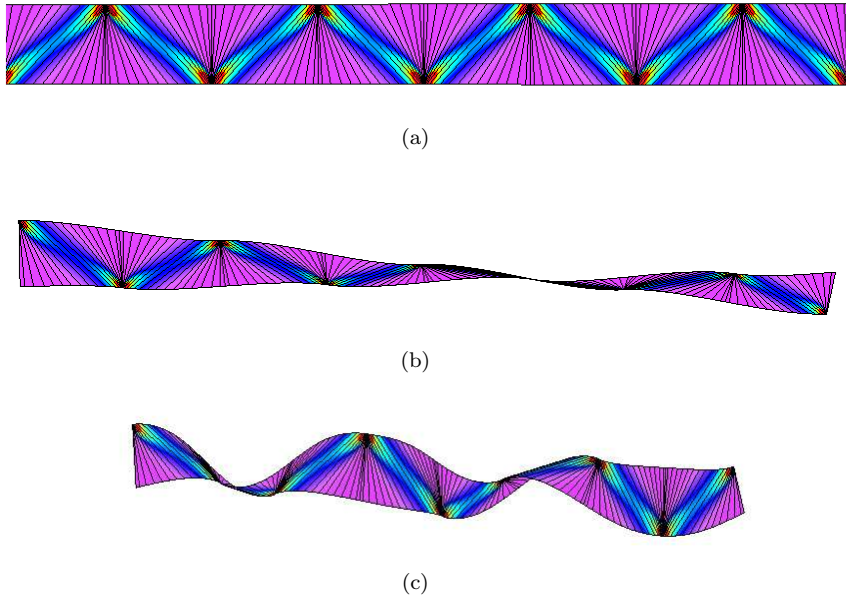


Figure 3: Shapes of strips for $n = 8$. (a) $\bar{F} = 13.42$, $\bar{M} = 0.162$. (b) $\bar{F} = 6.80$, $\bar{M} = 2.71$. (c) $\bar{F} = 0.197$, $\bar{M} = 12.15$.

solutions of a given period from solutions of another different period, with the same aspect ratio, via a w continuation. For example, starting from a strip of length $2nL$, width $2w$, and period $n = 2m$, selecting $n/2$ consecutive periods gives a strip of length nL , continuing this solution to w and rescaling $s \rightarrow 2s$ gives a period $n/2$ strip with the same aspect ratio as the original strip. All strips are scaled to an aspect ratio of $2nL/2w = 10.5300$ unless otherwise stated.

Many different strip shapes are obtained depending on the boundary conditions (2.16). In figure 3 are shown three shapes of a strip with $n = 8$, one under a high axial tension, one under a relatively high axial moment and an intermediate one which is in reasonably good agreement with the experiment in figure 1(a). Here, and in all surface plots in this paper, the colouring varies according to the bending energy density, from violet for regions of low bending to red for regions of high bending (scales are individually adjusted).

Continuation results for modes $n = 2, 4, 8$ are shown in figures 4–6 (for aspect ratio $2nL/2w = 10.5300$, except for figure 6(a), which has aspect ratio 42.30). On the left of each figure is shown the force response for the sequence of axial moments (\bar{M}) shown on the legend. The length scale is arbitrary and is such that $L = 0.6581$. On the right of each figure is shown the moment response for the sequence of axial forces (\bar{F}) shown on the legend. These curves were obtained by continuation, where \bar{F} was varied, keeping \bar{M} fixed or vice versa. Exceptions to this are some curves in figure 5(a,b) and figure 6(a), where both \bar{F} and \bar{M} were allowed to vary, only so that a continuation could be started at an arbitrary point on the graph (at which point one of \bar{F}, \bar{M} would then be held fixed). This accounts for the curve-crossing in this figure.

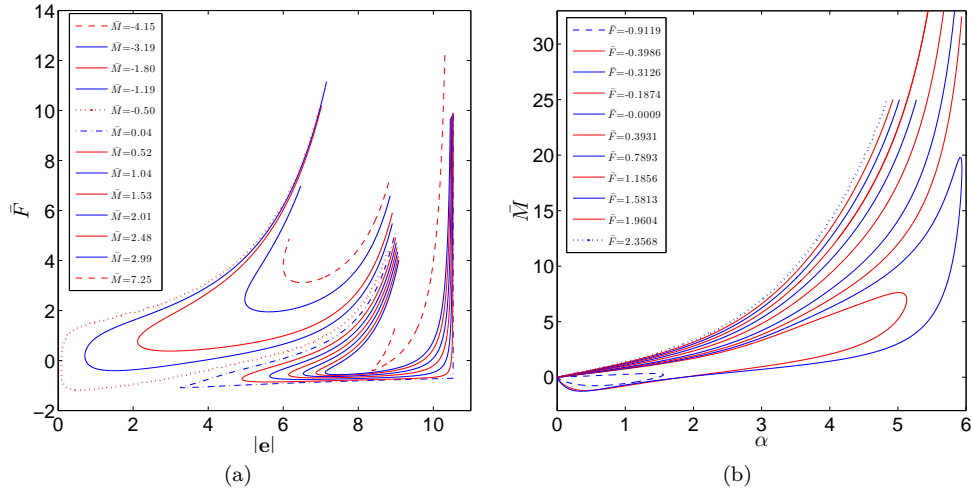


Figure 4: $n = 2$ mode. (a) Force \bar{F} versus scaled end-to-end distance, $|e|$. The curves of constant \bar{M} form a nested sequence on the plot, with \bar{M} increasing from the top middle dashed curve ($\bar{M} = -4.15$) to the dotted curve, then from the dot-dashed curve to the dashed curve on the right. (b) Moment \bar{M} versus twist angle α (in radians). The curves of constant \bar{F} form a nested sequence on the plot, with \bar{F} increasing from the dashed curve ($\bar{F} = -0.9119$) to the dotted curve.

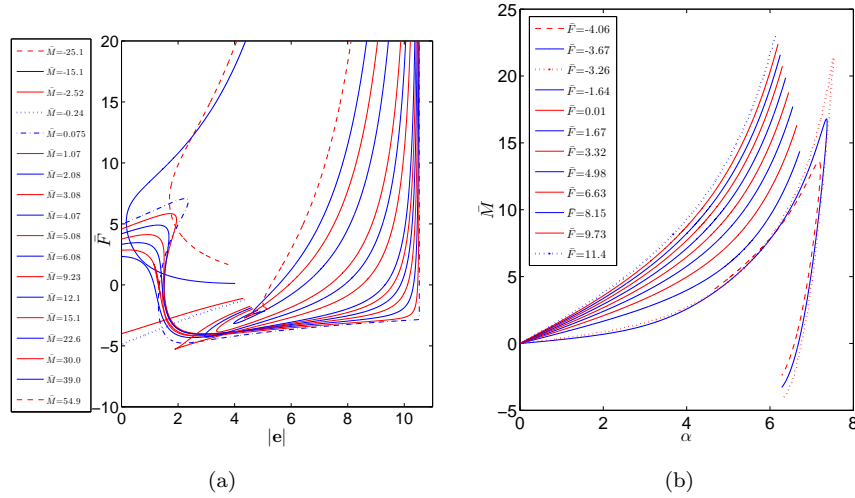


Figure 5: $n = 4$ mode. (a) Force \bar{F} versus scaled end-to-end distance, $|e|$. The curves of constant \bar{M} form a sequence on the plot, with \bar{M} increasing from the top left dashed curve ($\bar{M} = -25.1$) to the dotted curve, then from the dot-dashed curve to the top right dashed curve. (b) Moment \bar{M} versus twist angle α (in radians). The curves of constant \bar{F} form a sequence on the plot, with \bar{F} increasing from the dashed curve ($\bar{F} = -4.06$) to the dotted curve ($\bar{F} = -3.26$), then to the top dotted curve.

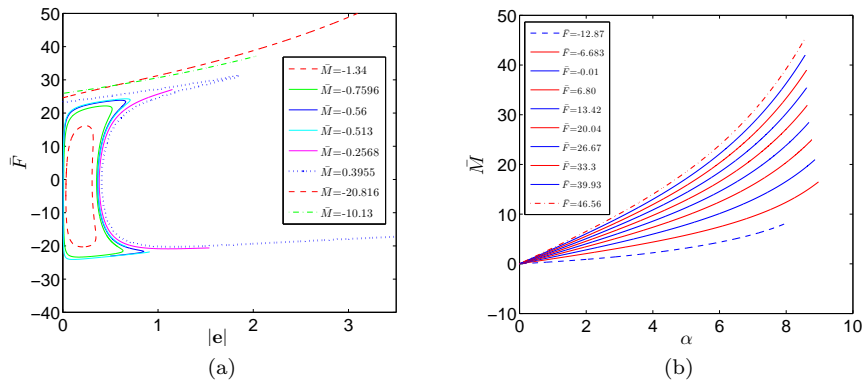


Figure 6: $n = 8$ mode. (a) Force \bar{F} versus scaled end-to-end distance, $|e|$. The curves of constant \bar{M} form a nested sequence on the plot, with \bar{M} increasing from the left dashed loop ($\bar{M} = -1.34$) to the dotted curve, then from the dot-dashed curve to the top dashed curve. (b) Moment \bar{M} versus twist angle α (in radians). The curves of constant \bar{F} form a nested sequence on the plot, with \bar{F} increasing from the dashed curve ($\bar{F} = -12.87$) to the dot-dashed curve.

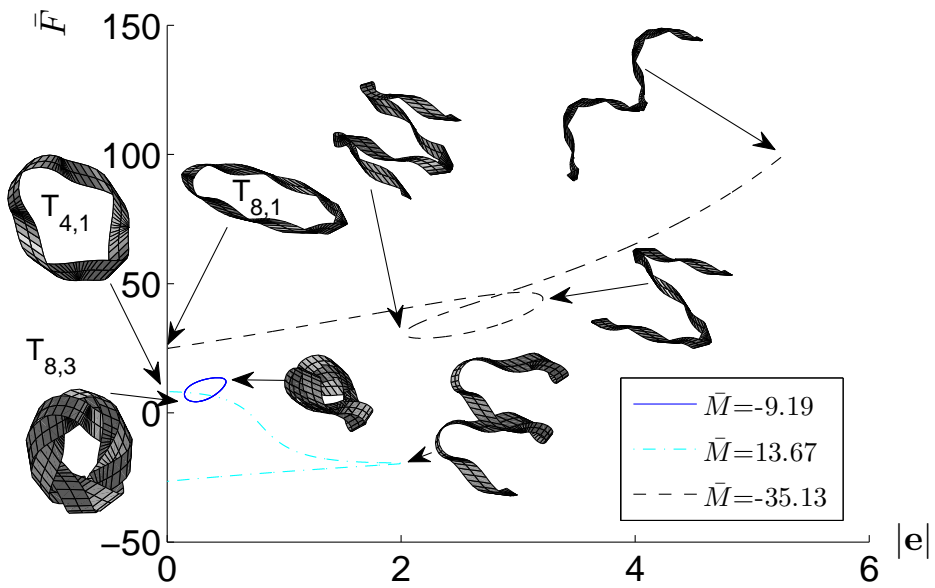


Figure 7: $n = 8$ mode. Force \bar{F} versus scaled end-to-end distance, $|e|$, showing strip solutions.

In figure 4(a), for the $n = 2$ mode, the sequence of curves at constant negative applied end moment is the group at the bottom left, with the moment increasing from top (large negative) to bottom (near zero). The group of curves at the bottom

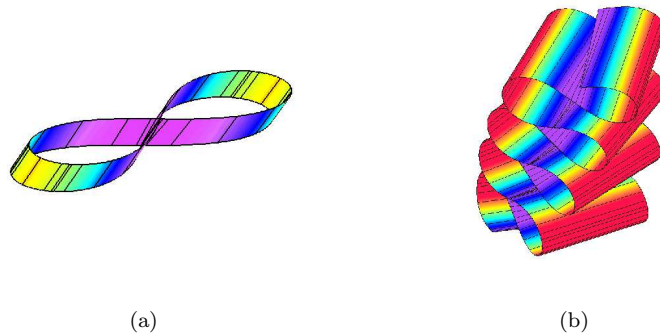


Figure 8: Shapes of strips. (a) $n = 2$, figure-of-eight. (b) $n = 8$, $\bar{F} = -19.975$, $\bar{M} = 0.1424$.

right of the figure is for constant positive applied end moment, with the moment increasing from bottom (near zero) to top (large positive). In figure 4(b) is a sequence of curves at constant applied end force, increasing from bottom (negative) to top (positive). The curves for smallest (negative) constant force start at zero moment, have a maximum twisting angle, which returns to zero twist angle, which is the figure-of-eight shown in figure 8(a).

In figure 5(a), for the $n = 4$ mode, the sequence of curves at constant negative applied end moment is the group at the bottom left, with the moment increasing from top (large negative) to bottom (near zero). The group of curves at the bottom right of the figure is for constant positive applied end moment, with the moment increasing from bottom (near zero) to top (large positive). In figure 5(b) is a sequence of curves at constant applied end force, increasing from bottom (negative) to top (positive), showing the response curve of applied end moment to the twist angle α . The three lowest negative applied force continuations terminate at $\alpha = 2\pi$, again forming a closed strip, this time the $T_{4,1}$ elastic torus ribbon knot.

In figure 6(a), for the $n = 8$ mode, is a sequence of curves at constant applied end moment (positive and negative). This picture is more complicated than the other modes. Some of the curves terminate on the vertical axis, i.e., when the end-to-end distance vanishes. These closed ribbon solutions are invariably torus ribbon knots. For example, the upper dashed curve ($\bar{M} = -20.816$) terminates in the double cover of the $T_{4,1}$ elastic torus ribbon knot. The series of nested closed curves have a quadruple cover of the figure-of-eight solution where the curves approach vanishing end-to-end distance. In figure 6(b) is a sequence of curves at constant applied end force, increasing from bottom (negative) to top (positive), showing the response curve of applied end moment to the twist angle α .

In figure 7, for the $n = 8$ mode, is a sequence of curves at constant applied end moment, with some of the resulting structures shown. The upper curve ($\bar{M} = -35.13$) terminates in the $T_{8,1}$ elastic torus ribbon knot. Both ends of the dot-dashed curve ($\bar{M} = 13.67$) terminate in a double covering of the $T_{4,1}$ elastic torus ribbon knot, whereas the $T_{8,3}$ structure (shown at the minimum end-to-end distance of the loop) does not quite close, as can be seen by the fact that the curve from which it originates does not meet the vertical axis. The other structure shown on

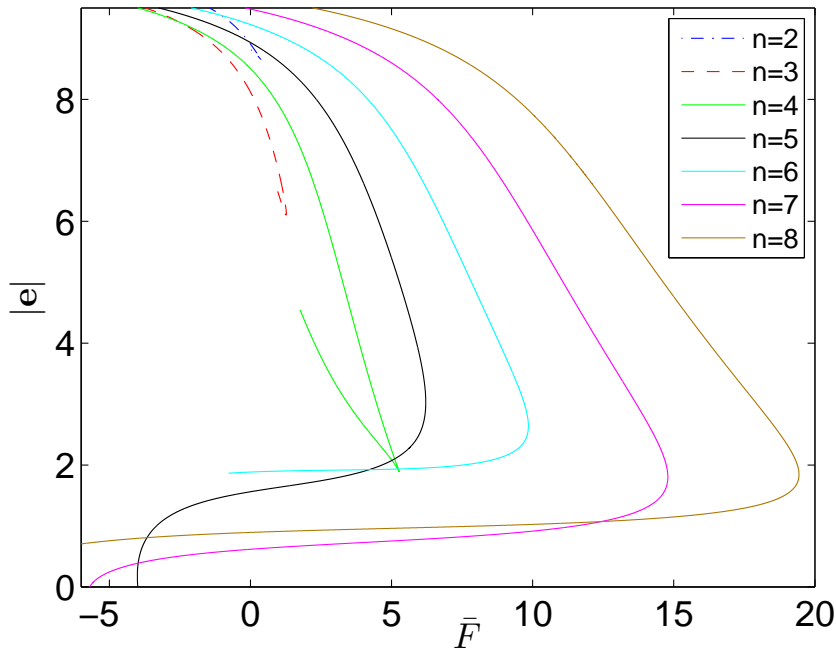


Figure 9: Fold structure of scaled end-to-end distance versus applied force \bar{F} , $n = 2, \dots, 8$ at constant $\bar{M} = 14.49$.

the same loop in the line diagram (shown at the maximum end-to-end distance of the loop on the figure) is related to the $T_{8,3}$ torus knot, but it is also not closed, and moreover the surface of the strip is self-intersecting.

As an example of further strip solutions, in figure 8(b) is shown a solution, with $n = 8$ and under a compressive axial force, that is not located on any of the computed response curves.

Figure 9 displays force-extension curves for varying mode number, $n = 2, \dots, 8$, at fixed moment \bar{M} . To obtain this plot, strips for different modes have been scaled to the same aspect ratio $2nL/2w = 10.5300$. Parts of these curves with positive slope are expected to correspond to stable solutions. The curves predict that, for $n \geq 5$, under increasing tension solutions jump to higher mode (down in $|e|$) as the force is increased beyond the folds seen in the diagram.

4. Discussion

When twisted, and pulled, an acetate model strip buckles into a regular pattern of triangular facets. We have computed periodic solutions describing this buckling pattern by formulating and numerically solving a geometrically-exact boundary-value problem for the large deformation of a thin, wide, inextensible strip. We have also obtained response curves of force against end-to-end distance and twisting moment against end-to-end angle for mode numbers $n = 2, 4$ and 8 . Our results predict

critical forces and jumps into higher buckling modes that would be interesting to explore experimentally.

By construction our solutions are periodic, which tends to be what one observes in experiments. However, non-periodic solutions can be constructed in a similar way by matching different trapezoidal segments. One would keep the first symmetry operation (reflection about the normal at the cylindrical point) but instead of reflecting about the binormal at the inflection point in the second step one could match the segment to a (suitably rescaled) trapezoidal segment of different length L . The resulting solution would no longer be symmetric about the inflection points.

In Mansfield (1989) and Ashwell (1962) analyses were performed similar to ours in that there too the double strain energy integral was reduced by integrating along the generator. However, the integrand expression was subsequently simplified by using an approximate moment balance equation that ignores the non-planarity of the strip. This approach gives a realistic evolution of the generator with arclength, but fails to predict the appearance of a cylindrical point at finite distance from the clamped end of the strip.

Triangular patterns are known to occur in a variety of problems of elastic sheets, including fabric draping and paper crumpling (Witten 2007). A sheet crumples (forming sharp points and straight creases) when it is forced into a constrained area. The sheet is predominantly under compression. It is interesting to note that, by contrast, in our triangular buckling pattern the strip is in (relatively high) tension. In both cases we observe a focussing of the strain energy which may lead to fracture of the material. Strain energy localisation thus appears to be a generic response of a thin elastic sheet to an external constraint.

Our results may be relevant for paper, fabric and sheet metal processing. They may also be of importance in the robotic manipulation of flexible belts, e.g., film circuit boards (Wakamatsu *et al.* 2007). In all these sheet manipulations it is important to avoid shapes with high concentrated stresses that may lead to tearing. Our formulation may help to choose boundary conditions that avoid unwanted configurations.

This work was supported by the UK's Engineering and Physical Sciences Research Council (EPSRC) under grant no. EP/F023383/1.

Appendix A. Derivation of the equations using standard variational techniques

We wish to calculate the variation of the functional $H = \int f(\kappa, \tau, \kappa', \tau') ds$. This calculation can be done using the formulation of Capovilla *et al.* (2002), substituting explicit expressions for quantities wherever they arise and grouping similar terms, which gives fully simplified expressions for all quantities of interest.

Alternatively, one can re-use the variations already calculated in Capovilla *et al.* (2002), to yield the same results, without having to compute new variations. There, for example, the variation is given for $H_1 = \int f_1(\kappa, \tau) ds$, stating that it can be written down from the variations of $H_2 = \int f_2(\kappa) ds$ and $H_3 = \int f_3(\tau) ds$, which are previously calculated. The resulting force and moment corresponding to H_1 can then be written down from the expressions for the force and moment for H_2 and H_3 . This follows from the chain rule. Similarly, one can calculate the variation of

the functional $H = \int f(\kappa, \tau, \kappa', \tau') ds$ using δH_1 without computing new variations. This follows as a consequence of the chain and product rules in differentiation. The resulting force and moment corresponding to H can then be written down from the expressions for the force and moment for H_1 , with a small number of additional terms arising from the chain and product rules.

Instead of following these approaches, we here use a third and more economical method by leaving δH expressed in terms of $\delta\kappa$ and $\delta\tau$ only. This method is easily generalised to functionals involving higher derivatives of κ and τ . Following the notation of Capovilla *et al.* (2002), the infinitesimal deformation of a space curve is $\delta\mathbf{r} = \Psi_{||}\mathbf{t} + \Psi_1\mathbf{n} + \Psi_2\mathbf{b}$, and denoting $\delta_{||}, \delta_{\perp}$ as the tangential and normal parts of the deformation respectively, the variation of any functional $H = \int f ds$ is

$$\delta H = \delta_0 H + \int \delta_{\perp} f ds, \quad (\text{A } 1)$$

where $\delta_0 H \equiv \delta_{||} H + \int f \delta_{\perp} ds = \int ((f\Psi_{||})' - f\kappa\Psi_1) ds$.

We therefore need to calculate the second term on the right-hand side of equation (A 1), where by the chain rule, $\delta_{\perp} f = f_{\kappa}\delta_{\perp}\kappa + f_{\tau}\delta_{\perp}\tau + f_{\kappa'}\delta_{\perp}\kappa' + f_{\tau'}\delta_{\perp}\tau'$, using the notation $f_{\beta} \equiv \partial f/\partial\beta$. Since for any scalar h , $\delta_{\perp}(h') = \kappa h'\Psi_1 + (\delta_{\perp}h)'$, then

$$\delta_{\perp} f = (f_{\kappa} - f'_{\kappa'})\delta_{\perp}\kappa + (f_{\tau} - f'_{\tau'})\delta_{\perp}\tau + \kappa(\kappa'f_{\kappa'} + \tau'f_{\tau'})\Psi_1 + (f_{\kappa'}\delta_{\perp}\kappa + f_{\tau'}\delta_{\perp}\tau)', \quad (\text{A } 2)$$

where $\delta_{\perp}\kappa$ and $\delta_{\perp}\tau$ are given in Capovilla *et al.* (2002). Equation (A 1) along with equation (A 2) is of the form

$$\delta H = \int ds \mathcal{E}_i \Psi_i + \int ds \mathcal{Q}', \quad (\text{A } 3)$$

with \mathcal{Q} the Noether charge, so that the Euler-Lagrange equations $\mathcal{E}_i = 0$ can be immediately written down, since these are just the coefficients of Ψ_i which can be read off from equation (A 1). These are two coupled differential equations in the unknowns κ, τ , and the known density f , which are quoted in general form in Thamwattana *et al.* (2008) and in Hangan (2005) for the Sadowsky functional.

Apart from the Euler-Lagrange equations, it is of interest to find expressions for the conserved force \mathbf{F} and the moment \mathbf{M} . The force \mathbf{F} is obtained by specialising the deformation to a constant infinitesimal translation $\delta\mathbf{r} = \mathbf{e}$, where \mathbf{F} is defined by $\mathcal{Q} = -\mathbf{e} \cdot \mathbf{F}$. Similarly, the conserved moment \mathbf{T} is obtained by specialising the deformation to a constant infinitesimal rotation $\delta\mathbf{r} = \boldsymbol{\Omega} \times \mathbf{r}$, where \mathbf{T} is defined by $\mathcal{Q} = -\boldsymbol{\Omega} \cdot \mathbf{T}$ and decomposed into $\mathbf{T} = \mathbf{r} \times \mathbf{F} + \mathbf{M}$. Thus only the total derivative parts of (A 1) contribute to \mathbf{F} and \mathbf{M} . But these contributions can be read off from the results in Capovilla *et al.* (2002) by noting that a term in equation (A 2) of the form $a\delta_{\perp}b$, where $b = \kappa, \tau$, has to be re-expressed in the form (A 3) to isolate its total derivative part. This has already been done in Capovilla *et al.* (2002). For a term in equation (A 2) of the form $(a\delta_{\perp}b)'$, one just needs the contribution from $\delta_{\perp}b$.

Thus, for an infinitesimal rotation $\delta\mathbf{r}' = \boldsymbol{\Omega} \times \mathbf{r}' = \boldsymbol{\Omega} \times \mathbf{t}$ and $\delta\mathbf{r}'' = \kappa\boldsymbol{\Omega} \times \mathbf{n}$. Using the compact expressions of Langer & Perline (1991) (equations (3.7b,c)), $\delta\kappa = \delta\mathbf{r}'' \cdot \mathbf{n} - 2\kappa\delta\mathbf{r}' \cdot \mathbf{t}$ gives $\delta\kappa = 0$, i.e., $\delta_{\perp}\kappa = -\delta_{||}\kappa = -\Psi_{||}\kappa'$. But $\Psi_{||} \equiv \delta\mathbf{r} \cdot \mathbf{t} = (\mathbf{r} \times \mathbf{t}) \cdot \boldsymbol{\Omega}$, giving $\delta_{\perp}\kappa = -\boldsymbol{\Omega} \cdot (\kappa'\mathbf{r} \times \mathbf{t})$. As this is of the form $-\boldsymbol{\Omega} \cdot (\mathbf{r} \times \mathbf{F})$, $\mathcal{Q} \equiv a\delta_{\perp}\kappa$ in (A 2) does not contribute to the moment \mathbf{M} . Similarly, $\delta\tau = \delta\mathbf{r}'' \cdot \mathbf{b}/\kappa' + \delta\mathbf{r}' \cdot (\kappa\mathbf{b} - \tau\mathbf{t}) = 0$,

giving $\delta_{\perp}\tau = -\boldsymbol{\Omega} \cdot (\mathbf{r} \times \tau'\mathbf{t})$. As this is of the form $-\boldsymbol{\Omega} \cdot (\mathbf{r} \times \mathbf{F})$, $\mathcal{Q} \equiv a\delta_{\perp}\tau$ in (A 2) also does not contribute to the moment \mathbf{M} . (Note that by retaining these terms one would obtain the force \mathbf{F} , but in the next paragraph we will, instead, calculate \mathbf{F} by considering a constant infinitesimal translation.) Now, from Capovilla *et al.* (2002) (equations (49) and (67)), $a\delta_{\perp}\kappa$ contributes $-a\mathbf{b}$ to the moment, whereas $a\delta_{\perp}\tau$ contributes $-a\mathbf{t} - a'\mathbf{n}/\kappa$. Thus from equations (A 1) and (A 2) one can immediately write down the moment as:

$$\mathbf{M} = (f'_{\tau'} - f_{\tau})\mathbf{t} + (f''_{\tau'} - f'_{\tau})\mathbf{n}/\kappa + (f'_{\kappa'} - f_{\kappa})\mathbf{b}. \quad (\text{A } 4)$$

In order to calculate the contribution to the force of $\mathcal{Q} \equiv f_{\kappa'}\delta_{\perp}\kappa + f_{\tau'}\delta_{\perp}\tau$, one notes that since $\delta\mathbf{r} = \mathbf{e}$ is a constant, it follows from the formulation of Langer & Perline (1991) (equations (3.7b,c)) that $\delta\kappa = 0$, i.e., $\delta_{\perp}\kappa = -\delta_{\parallel}\kappa = -\Psi_{\parallel}\kappa' = -\mathbf{e} \cdot (\kappa'\mathbf{t})$. Thus the contribution of $\mathcal{Q} \equiv f_{\kappa'}\delta_{\perp}\kappa$ in (A 2) to \mathbf{F} is $\kappa'f_{\kappa'}\mathbf{t}$. In a similar manner, for this constant translation, $\delta\tau = 0$, giving $\delta_{\perp}\tau = -\mathbf{e} \cdot (\tau'\mathbf{t})$, so that $\mathcal{Q} \equiv f_{\tau'}\delta_{\perp}\tau$ in (A 2) contributes $\tau'f_{\tau'}\mathbf{t}$ to the force. Now from Capovilla *et al.* (2002) (equations (48) and (64)), $a\delta_{\perp}\kappa$ contributes $\kappa a\mathbf{t} + a'\mathbf{n} + \tau a\mathbf{b}$ to the force, whereas $a\delta_{\perp}\tau$ contributes $\tau a\mathbf{t} + \tau a'\mathbf{n}/\kappa - ((a'/\kappa)' + \kappa a)\mathbf{b}$. Also, $\delta_{\parallel}H$ contributes $-f\mathbf{t}$ to the force. Thus from equations (A 1) and (A 2) one can immediately write down the force as:

$$\begin{aligned} \mathbf{F} = & (-f + \kappa'f_{\kappa'} + \tau'f_{\tau'} + \kappa(f_{\kappa} - f'_{\kappa'}) + \tau(f_{\tau} - f'_{\tau'}))\mathbf{t} \\ & + \left(f'_{\kappa} - f''_{\kappa'} + \frac{\tau}{\kappa}(f'_{\tau} - f''_{\tau'}) \right)\mathbf{n} \\ & + \left(\tau(f_{\kappa} - f'_{\kappa'}) - \kappa(f_{\tau} - f'_{\tau'}) - ((f'_{\tau} - f''_{\tau'})/\kappa)' \right)\mathbf{b}. \end{aligned} \quad (\text{A } 5)$$

From these components of \mathbf{F} and \mathbf{M} , the differential equations for the moment components and the differential equation for F_t in equation (2.7) are easily obtained. For instance, from (A 4) it is seen that $M'_t = \kappa M_n$, while equations for M_n , M_b and F_t can be extracted similarly. The remaining two equations for F_n and F_b are obtained from (A 5) and the Euler-Lagrange equations $\mathcal{E}_i = 0$.

In summary, the variation of $H = \int f(\kappa, \tau, \kappa', \tau') ds$ can be easily obtained from the variations $\delta\kappa, \delta\tau$. Their explicit expressions are not required; their contributions can be read off from Capovilla *et al.* (2002). The additional terms generated by the additional dependence of f on κ' and τ' are therefore easily managed.

One way of regarding equations (A 4) and (A 5), is that they prescribe \mathbf{F} and \mathbf{M} once κ and τ for the given density f are known. The two Euler-Lagrange equations for κ and τ are given by $\mathcal{E}_i = 0$, i.e., by setting the coefficients of Ψ_i to zero in equation (A 3). Instead of solving the problem this way, however, it is preferable to set up an equivalent system of coupled one-dimensional ODEs as in Starostin & van der Heijden (2009). One way to do this is to use the natural variables \mathbf{F} and \mathbf{M} , and, for the functional (2.6), to change variables from (κ, τ) to (κ, η) .

By considering functionals of the form $g(\kappa, \eta, \eta') = f(\kappa, \tau, \kappa', \tau')$, one can show that $(\partial g/\partial\kappa)_{\eta, \eta'} = f_{\kappa} + \eta f_{\tau} + \eta' f_{\tau'}$, $(\partial g/\partial\eta)_{\kappa, \eta'} = \kappa f_{\tau} + \kappa' f_{\tau'}$ and $(\partial g/\partial\eta')_{\kappa, \eta} = \kappa f_{\tau'}$. Using these identities, and writing the components of the internal force \mathbf{F} and moment \mathbf{M} in the directions of the Frenet frame of tangent, principal normal and binormal as $\mathbf{F} = (F_t, F_n, F_b)^T$, $\mathbf{M} = (M_t, M_n, M_b)^T$, one can show, using the

tangent and binormal components of \mathbf{M} from equation (A 4), that

$$\begin{aligned} \partial_{\kappa}g + \eta M_t + M_b &= 0, \\ (\partial_{\eta'}g)' - \partial_{\eta}g - \kappa M_t &= 0. \end{aligned} \quad (\text{A } 6)$$

The two scalar equations, (A 6), along with the six balance equations (equation (2.7)) for the components of the internal force \mathbf{F} and moment \mathbf{M} (see Starostin & van der Heijden 2007, Starostin & van der Heijden 2009), are then the equations satisfied by the centreline of the developable strip for the unknowns $\mathbf{F}, \mathbf{M}, \kappa, \eta$:

$$\begin{aligned} \mathbf{F}' + \boldsymbol{\omega} \times \mathbf{F} &= \mathbf{0}, & \mathbf{M}' + \boldsymbol{\omega} \times \mathbf{M} + \mathbf{t} \times \mathbf{F} &= \mathbf{0}, \\ \partial_{\kappa}g + \eta M_t + M_b &= 0, & (\partial_{\eta'}g)' - \partial_{\eta}g - \kappa M_t &= 0, \end{aligned} \quad (\text{A } 7)$$

where $\boldsymbol{\omega} = \kappa(\eta, 0, 1)^T$ is the Darboux vector. Equations (A 7), (A 8) constitute a system of differential-algebraic equations that are turned into a system of ODEs by differentiation of the algebraic equation in (A 8).

References

- Anderson, I. M. 1989 *The Variational Bicomplex*. Technical report, Utah State University, Logan (available from http://www.math.usu.edu/~fg_mp/Publications/VB/vb.pdf).
- Doedel, E. J., Champneys, A. R., Fairgrieve, T. R., Kuznetsov, Y. A., Sandstede, B., & Wang, X. J. 2007 AUTO-07p: continuation and bifurcation software for ordinary differential equations (available from <http://indy.cs.concordia.ca/auto/>).
- Ashwell D. G. 1962 The inextensional twisting of a rectangular plate. *The Quarterly Journal of Mechanics and Applied Mathematics*, **15**:91–107.
- Capovilla, R., Chryssomalakos, C., & Guven, J. 2002 Hamiltonians for curves. *J. Phys. A: Math. Gen.*, **35**:6571–6587.
- Coman, C. D. & Bassom, A. P. 2008 An asymptotic description of the elastic instability of twisted thin elastic plates. *Acta Mechanica*, **200**:59–68.
- Crispino, D. J. & Benson, R. C. 1986 Stability of twisted orthotropic plates. *International Journal of Mechanical Sciences*, **28**:371–379.
- Goldstein, H. 1980 *Classical Mechanics*. Addison-Wesley Publishing Company, Inc..
- Graustein, W. C. 1966 *Differential Geometry*. New York: Dover.
- Green, A. E. 1936 The equilibrium and elastic stability of a thin twisted strip. *Proceedings of the Royal Society of London. Series A*, **154**:430–455.
- Green, A. E. 1937 The elastic stability of a thin twisted strip – II. *Proceedings of the Royal Society of London. Series A*, **161**:197–220.
- Hangan, T. 2005 Elastic strips and differential geometry. *Rend. Sem. Mat. Univ. Pol. Torino*, **63**:179–186.
- Hornung, P. 2009 Minimizers of Kirchhoff's plate functional: Euler-Lagrange equations and regularity. *C. R. Acad. Sci. Paris*, **347**:647–650.
- Kogan, I. A. & Olver, P. J. 2003 Invariant Euler-Lagrange equations and the invariant variational bicomplex. *Acta Applicandae Mathematicae*, **76**:137–193.
- Langer, J. & Perline, R. 1991 Poisson geometry of the filament equation. *J. Nonlinear Sci.*, **285**:131–144.
- Love, A. E. H. 1927 *A Treatise on the Mathematical Theory of Elasticity*. Cambridge University Press.
- Mansfield, E. H. 1989 *The Bending and Stretching of Plates*. Cambridge University Press, Cambridge, 2nd edition.

- Mockensturm, E. M. 2001 The elastic stability of twisted plates. *Journal of Applied Mechanics – Transactions of the ASME*, **68**:561–567.
- Randrup, T. & Røgen, P. 1996 Sides of the Möbius strip. *Arch. Math.*, **66**:511–521.
- Sadowsky, M. 1931 Theorie der elastisch biegsamen undehnbaren Bänder mit Anwendungen auf das Möbius'sche Band. *Verhandl. des 3. Intern. Kongr. f. Techn. Mechanik, 1930, Teil II*, pp. 444–451.
- Starostin, E. L. & van der Heijden, G. H. M. 2007 The shape of a Möbius strip. *Nat. Mater.*, **6**:563–567.
- Starostin, E. L. & van der Heijden, G. H. M. 2009 Force and moment balance equations for geometric variational problems on curves. *Phys. Rev. E*, **79**:066602.
- Thamwattana, N., McCoy, J. A., & Hill, J. M. 2008 Energy density functions for protein structures. *Quart. J. Mech. Appl. Math.*, **61**:431–451.
- van der Heijden, G. H. M. & Thompson, J. M. T. 2000 Helical and localised buckling in twisted rods: a unified analysis of the symmetric case. *Nonlinear Dynam.*, **21**:71–99.
- Wakamatsu, H., Yamasaki, T., Arai, E., & Hirai S. 2007 Modeling of flexible belt objects toward their manipulation. *Proceedings of the 2007 IEEE International Symposium on Assembly and Manufacturing*, pp. 1–6.
- Witten, T. A. 2007 Stress focusing in elastic sheets. *Rev. Mod. Phys.*, **79**:643–675.
- Wunderlich, W. 1962 Über ein abwickelbares Möbiusband. *Monatsh. Math.*, **66**:276–289.
- Yoshimura, Y. 1951 *On the mechanism of buckling of a circular cylindrical shell under axial compression and bending*. Reports of the Institute of Science and Technology of the University of Tokyo, vol. 5(5), (English translation: Technical Memorandum 1390 of the National Advisory Committee for Aeronautics, Washington DC, 1955).